Observations of dark and luminous matter: the radial distribution of satellite galaxies around massive red galaxies

The Astrophysical Journal Letters, 751:L5 (6pp), 2012 May 20 doi:10.1088/2041-8205/751/1/L5

OBSERVATIONS OF DARK AND LUMINOUS MATTER: THE RADIAL DISTRIBUTION OF SATELLITE GALAXIES AROUND MASSIVE RED GALAXIES

Tomer Tal, David A. Wake, and Pieter G. van Dokkum
Astronomy Department, Yale University, P.O. Box 208101, New Haven, CT 06520-8101, USA; tomer.tal@yale.edu
Received 2012 January 24; accepted 2012 April 12; published 2012 April 30

ABSTRACT

We study the projected radial distribution of satellite galaxies around more than 28,000 luminous red galaxies (LRGs) at $0.28 < z < 0.40$ and trace the gravitational potential of LRG groups in the range $15 < r/\mathrm{kpc} < 700$. We show that at large radii the satellite number-density profile is well fitted by a projected Navarro–Frenk–White (NFW) profile with $r_s \sim 270$ kpc and that at small radii this model underestimates the number of satellite galaxies. Utilizing the previously measured stellar light distribution of LRGs from deep imaging stacks, we demonstrate that this small-scale excess is consistent with a non-negligible baryonic mass contribution to the gravitational potential of massive groups and clusters. The combined NFW+scaled stellar profile provides an excellent fit to the satellite number-density profile all the way from 15 kpc to 700 kpc. Dark matter dominates the total mass profile of LRG halos at $r > 25$ kpc whereas baryons account for more than 50% of the mass at smaller radii. We calculate the total dark-to-baryonic mass ratio and show that it is consistent with measurements from weak lensing for environments dominated by massive early-type galaxies. Finally, we divide the satellite galaxies in our sample into three luminosity bins and show that the satellite light profiles of all brightness levels are consistent with each other outside of roughly 25 kpc. At smaller radii we find evidence for a mild mass segregation with an increasing fraction of bright satellites close to the central LRG.

Key words: dark matter – galaxies: elliptical and lenticular, cD – galaxies: groups: general

Online-only material: color figures

1. INTRODUCTION

Measurements of the mass profile of galaxy groups and clusters hold key insight into the distribution of dark and baryonic matter in galaxy environments. Such analyses are difficult to perform observationally as the gravitational potential of massive environments is predicted to be dominated by dark matter halos. Therefore, significant efforts have been devoted to indirect measurements, such as observations of the hot interstellar medium and the dynamics of satellite galaxies in groups and clusters (e.g., Fabricant et al. 1980; Forman & Jones 1982; Mulchaey et al. 1993; Girardi et al. 1993; Fadda et al. 1996; Vikhlinin et al. 2006). Other indirect approaches, such as galaxy clustering and gravitational lensing, successfully measure the distribution of mass through its effect on other mass concentrations (e.g., Vader & Sandage 1991; Zehavi et al. 2002; Madore et al. 2004; Mandelbaum et al. 2006; Masjedi et al. 2006, 2008; Gavazzi et al. 2007; Bolton et al. 2008; Wake et al. 2008; Watson et al. 2011).

One such method utilizes measurements of the radial number-density profile of satellite galaxies to trace the underlying gravitational potential of group or cluster halos. This approach is challenging as it requires identifying galaxies as satellites and separating them from other objects along the line of sight. Accurate identifications of satellites using spectroscopic redshifts are observationally expensive and are restricted to the brightest galaxies.

Alternatively, one can measure the radial number-density profile of satellite galaxies in a statistical manner, in effect stacking results from a large number of groups and clusters in a well-defined sample. This method can provide a measurement of the total mass profile at essentially all relevant scales but requires large-scale homogeneous imaging samples such as that provided by the Sloan Digital Sky Survey (SDSS; York et al. 2000).

Throughout the Letter we adopt the following cosmological parameters: $\Omega_m = 0.3$, $\Omega_\Lambda = 0.7$, and $H_0 = 70\ \mathrm{km\ s^{-1}\ Mpc^{-1}}$.

2. DATA AND ANALYSIS

We selected galaxy images for this study from the seventh data release of SDSS (Abazajian et al. 2009) using the criteria presented in Tal et al. (2012). This sample includes the reddest, most luminous red galaxies (LRGs) at redshift $0.28 < z < 0.4$ with rest-frame g-band magnitudes brighter than -22.42 and rest-frame $g - r$ color values redder than 0.74. These are the most massive galaxies in the nearby universe with total stellar masses greater than a few times $10^{11}\ M_\odot$. More than 90% of the selected LRGs are expected to be the central galaxies in their halos and are thought to be residing in groups with typical total masses of a few times $10^{13}\ M_\odot$ (Wake et al. 2008; Zheng et al. 2009; Reid & Spergel 2009). The final data set includes 28,017 LRGs for which we acquired r-band images from the SDSS archive.

In order to extract the radial distribution of satellite galaxies in LRG environments we followed a statistical approach to remove the contamination of foreground and background objects from the LRG fields. We started by subtracting the LRG light from each image using a fourth-order radial b-spline model, utilizing the IDLUTIL package (Bolton et al. 2006). Next, we used SExtractor (Bertin & Arnouts 1996) to detect all objects in an annulus of radius 150″ (720 kpc at $z = 0.34$) around the LRGs, utilizing a detection threshold of 2σ above the background. We measured the projected physical distance between each detected object and the central LRG, assuming that all sources are at the same redshift as the LRG. We then combined the results from all fields and divided them into radial bins. Finally, we performed an

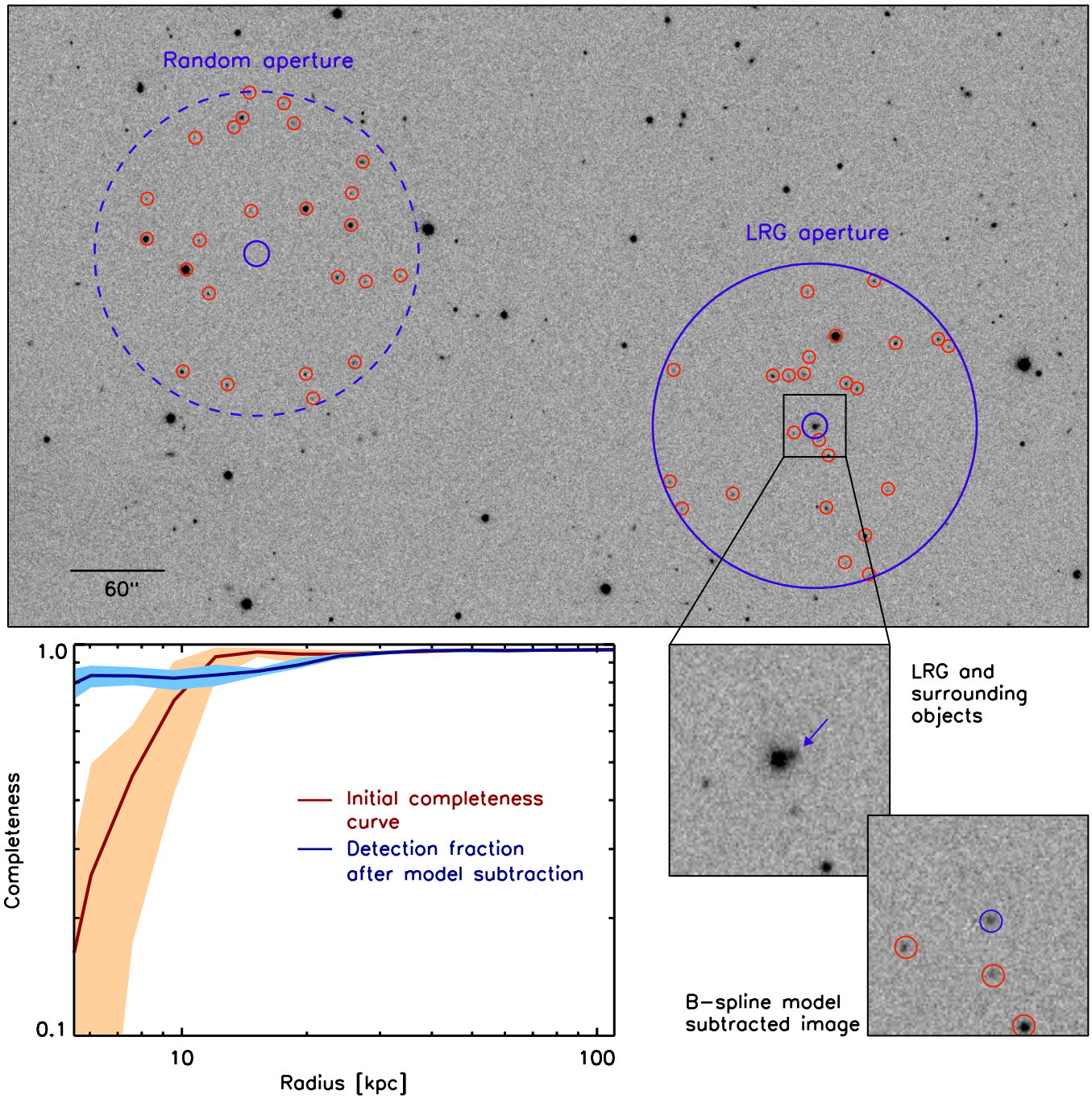

Figure 1. Top panel: illustration of the satellite radial profile extraction technique. Objects are identified in annuli around the LRG (red circles) and projected distances are measured from the central galaxy. An identical analysis is then performed in randomly positioned apertures along the same SDSS fields and object distances are measured to the center of the random aperture. After combining the measurements of more than 28,000 apertures we subtracted the contribution of foreground and background sources from the radial profile of objects in LRG environments. Bottom right: upon subtraction of a b-spline model fit to the central LRG, additional objects may be detected at small projected radii (blue arrow and blue circle). Bottom left: completeness tests using mock galaxies show that model fitting and subtraction uncovers a large fraction of satellite galaxies at small projected radii. The blue and orange curves represent the distribution of completeness levels for the full satellite brightness range for galaxies modeled with a Sérsic profile with $n = 2.5$ and $r_e = 4$ kpc.

(A color version of this figure is available in the online journal.)

identical source extraction in 10 randomly positioned apertures along each of the SDSS fields and measured projected distances to the aperture centers. An illustration of the measurement technique is presented in Figure 1.

The number density of objects detected in the proximity of any bright source typically underestimates the true number of sources in that region. To quantify the success rate of object detection close to the LRGs we randomly positioned five mock galaxy images in each SDSS frame and repeated the analysis portrayed in Section 2. We modeled these galaxies using a Sérsic light profile with index $n = 2.5$, effective radius $r_e = 4$ kpc, and total brightness between 18.7 and 21.3 mag. The bottom left panel of Figure 1 shows the detection fraction of mock galaxies from the LRG fields before and after subtracting the best-fitting b-spline model. We derived a correction factor from the running median of the model-subtracted curve (blue line in Figure 1) to

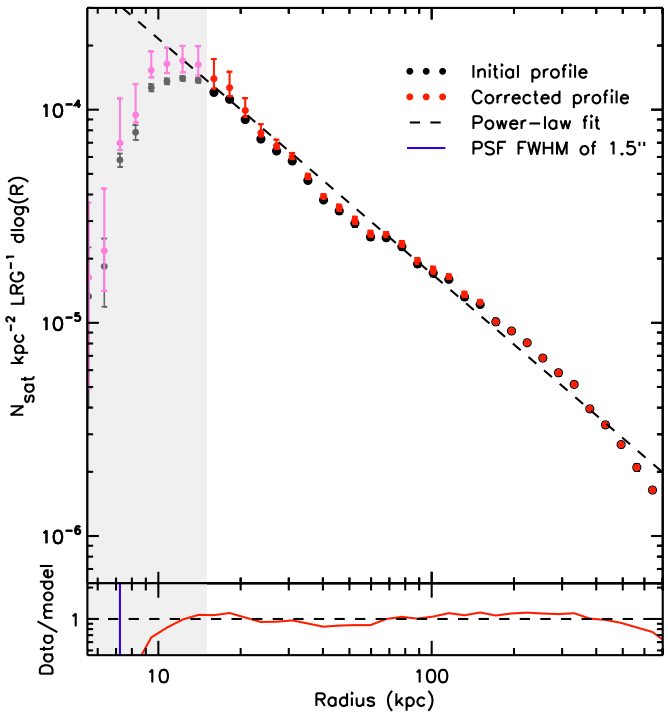

Figure 2. Projected number-density profile of satellite galaxies around LRGs at $z = 0.34$. The black points show the radial distribution of sources after a statistical subtraction of foreground and background objects. The red points represent the same distribution after a correction factor was applied to account for incompleteness. At $15 < r/\mathrm{kpc} < 700$ the profile is reasonably well fitted by a single power-law model with a slope of -1.1 and residuals of up to roughly 20% (dashed line). Data points inside of the fitting radius (15 kpc) are marked by a shaded region and the full width at half-maximum of typical SDSS stellar point-spread function is represented by a blue line.

(A color version of this figure is available in the online journal.)

account for missing objects due to incompleteness. In addition to demonstrating a high completeness rate of more than 80% at projected $r > 6$ kpc, this figure shows the efficiency of b-spline model fitting at characterizing the central galaxy light at all radii (in agreement with results by Bolton et al. 2006; Nierenberg et al. 2011).

3. RESULTS

The resulting projected number-density profile of satellite galaxies around LRGs is shown in Figure 2. Black points represent the "raw" difference between counts in LRG fields and in random fields and red points are corrected for incompleteness (see Section 2). We show the profile for all sources that are brighter than 21.3 mag, which is roughly 3 mag fainter than the mean LRG brightness.

In order to assess the errors in the measured profile we calculated the standard deviation of the distribution of random aperture measurements in each radial bin. In addition, we repeated the completeness calculation that is described in Section 2 for galaxies modeled with Sérsic parameters between $1 < n < 4$ and between $2 < r_e/\mathrm{kpc} < 6$, with total brightness between 18.7 and 21.3 mag. The range of completeness correction factor values represents a potential systematic error which is driven by the possible spread of satellite galaxy properties around the studied LRGs. The error bars in Figure 2 fold in the uncertainties from both of the above-mentioned potential error sources.

The projected number-density profile of LRG satellite galaxies is confidently traced in the range $15 < r/\mathrm{kpc} < 700$. At radii larger than roughly 15 kpc, the profile declines monotonically while at smaller radii the slope is positive. Figure 2 shows that in the range $15 < r/\mathrm{kpc} < 700$ the profile is relatively well fitted by a single power-law model of the form $\log N_{\mathrm{sat}} = -1.1 \log r + 2.7 \times 10^{-3}$ (dashed line) with residuals of up to roughly 20% (bottom panel). The gray line in Figure 2 shows the full width at half-maximum of the typical stellar point-spread function.

4. MODEL FITTING

The power-law fit presented in Figure 2 provides a reasonable description of the projected number-density profile of LRG satellites. Nevertheless, the residuals from this fit (bottom panel of Figure 2) suggest that this model may not best represent the projected total mass distribution in LRG environments. A more physically motivated model for this may be the Navarro–Frenk–White (NFW) profile (Navarro et al. 1996, 1997), which provides a good approximation of the radial density distribution of dark matter halos. In the following subsections we test how well the NFW model fits the satellite galaxy number-density profile.

4.1. NFW Profile Fit

Following Bartelmann (1996) we write the analytical approximation of the projected NFW profile as

$$\Sigma(x) \propto \begin{cases} (x^2-1)^{-1}\left(1 - \frac{2}{\sqrt{x^2-1}}\arctan\sqrt{\frac{x-1}{x+1}}\right) & (x > 1) \\ 1/3 & (x = 1) \\ (x^2-1)^{-1}\left(1 - \frac{2}{\sqrt{1-x^2}}\mathrm{arctanh}\sqrt{\frac{1-x}{1+x}}\right) & (x < 1) \end{cases}, \quad (1)$$

where $x \equiv r/r_s$ and r_s is the scale radius. We used the nonlinear least-squares curve fitting program MPFIT (Markwardt 2009) to fit the above approximation of the projected NFW model to the satellite number-density profile. We allowed both model parameters (r_s and the normalization factor) to be fitted, in practice allowing the fit to be arbitrarily normalized. The left panel of Figure 3 shows that a single NFW profile (black dotted line) fails to describe the full range of the number-density profile (red points) better than the power-law model. This is especially relevant on small scales ($r < 25$ kpc), where the projected NFW model underpredicts the number of satellite galaxies by up to a factor of two (bottom left panel). Assuming that the number-density profile traces the total mass in LRG halos, this may suggest that an additional component contributes to the gravitational potential on small scales.

4.2. NFW+Sérsic

Although baryons are predicted to contribute only a small fraction of the total mass of massive halos, they are more concentrated than the dark matter halos with stellar half-light radii of roughly 10 kpc. This implies that on small scales the gravitational potential of LRG groups and clusters may be dominated by baryons, whose distribution does not necessarily follow an NFW profile.

To test this we utilized the surface brightness profile of a deep imaging stack of more than 40,000 $z = 0.34$ LRGs from Tal & van Dokkum (2011). The stacked light profile portrays the distribution of luminous matter in the galaxy and it is well fitted by a single Sérsic model in the range $1 < r/\mathrm{kpc} < 100$. We utilized the best-fit Sérsic parameters from the stacking

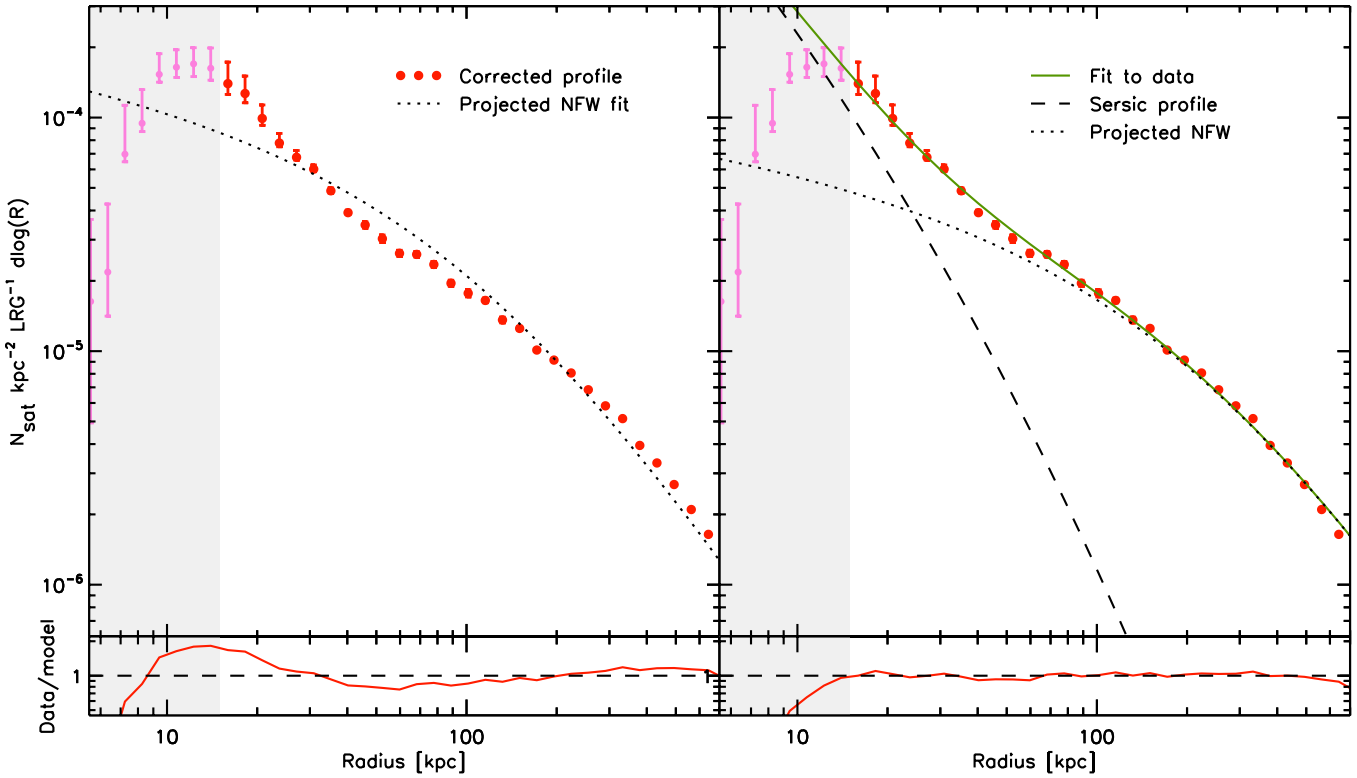

Figure 3. Model fitting to the projected number-density profile of satellite galaxies around LRGs. Left panel: the overall profile (red data points) is poorly fitted by a single projected NFW model (black dotted line) with residuals of up to roughly 100%. Right panel: an NFW+Sérsic model fit to the profile in the range $15 < r/\mathrm{kpc} < 700$. At large radii, the profile is well fitted by a single projected NFW model (black dotted line); when combined with an arbitrarily normalized Sérsic model (black dashed line; n and r_e taken from a fit to the light profile of deep imaging stack of the same LRGs), the fit to the number-density profile is excellent (green solid line). The shaded region marks the minimum fitting radius in both panels.

(A color version of this figure is available in the online journal.)

analysis ($n = 5.5$ and $r_e = 13.1$ kpc) to fit the satellite number-density profile with an NFW+Sérsic function. This fit has three free parameters: the NFW scale radius r_s and independent normalizations for each of the two model components.

The upper right panel of Figure 3 shows the best-fit NFW+Sérsic model (green line) to the number-density profile (red points). The bottom right panel of the figure shows that this model provides an excellent description of the projected number-density profile with fit residuals of less than 10%. At large radii the profile is well fitted by an NFW model with $r_s = 267 \pm 6$ kpc (black dotted line) while at small radii the excess number of satellites is dominated by the Sérsic model (black dashed line). The error bars in Figure 3 fold in the same uncertainties as those discussed in Section 3 and they show that the shape of the satellite number-density profile depends only mildly on the satellite galaxy properties.

Finally, we note that for a typical LRG group halo mass of $5 \times 10^{13}\,M_\odot$ the best-fit scale radius implies a concentration parameter $c \equiv r_{200}/r_s \sim 2$. The quoted uncertainty in the value of r_s is simply the formal 1σ fitting error and does not account for systematic errors. We discuss the effect of such systematic uncertainties in Section 5.4.

5. DISCUSSION

5.1. Ratio of Dark to Luminous Matter

The excellent agreement between the projected number-density profile of satellite galaxies around LRGs and an NFW+Sérsic model suggests that the contribution of baryonic mass is non-negligible in the inner regions of such groups and clusters. Assuming that the satellite profile traces the total mass distribution we can utilize the functional fits to estimate the ratio between dark and baryonic mass in LRG environments. To do so we separately integrated the two components of the best-fit NFW+Sérsic model out to 700 kpc and calculated the area under the curves, resulting in a total dark-to-baryonic mass ratio of 80. If we further assume that stars typically account for only half of the baryonic mass in galaxy groups (Mulchaey 2000) then the implied baryon conversion factor, $\eta = 0.037$, is consistent with the weak-lensing result from Mandelbaum et al. (2006) for massive early-type galaxies.

The high fraction of baryonic mass in LRG groups may suggest that LRGs represent an extreme population of galaxies, where a large fraction of the stellar mass in the halo had been incorporated into the central galaxy. This is in agreement with Tal et al. (2012) who found that roughly 35% of the stellar mass in LRG groups is locked in the LRG itself. Recent numerical and observational studies of satellites around central galaxies with a broader range of properties find a less pronounced deviation from a projected NFW profile (van den Bosch et al. 2005; Sales et al. 2007; Guo et al. 2012).

5.2. Small-scale Number-density Profile

Throughout the analysis of the number-density profile we utilized a lower radius limit for the functional fits in order to avoid the inner part of the profile at $r < 15$ kpc. At small radii the number density of satellite galaxies drops dramatically despite a high expected detection fraction (as predicted by the

completeness curve of Figure 1). We consider two plausible scenarios to explain this change in profile slope: a deficit of satellite galaxies due to interactions with the LRG and an underestimate of the true number of satellites due to detection limits.

The turnover point of the profile slope is at roughly 15kpc, only about 2 kpc farther out than the average half-light radius of LRGs (13.1 kpc; Tal et al. 2012). In such proximity to the massive central, satellite galaxies experience strong tidal forces and possibly ram-pressure stripping, both acting to remove mass from the infalling galaxies. It is possible that many satellite galaxies below a certain mass threshold do not survive for long close to the halo center and that their stars are quickly incorporated into the LRG itself.

Alternatively, our simulations may underestimate the effects of incompleteness close to the LRG itself. However, we note that the deficiency of satellites at small radii cannot be caused by simple signal-to-noise ratio effects as this deficiency seems to be strongest for the brightest galaxies (see below). To test this, imaging of higher spatial resolution and a more accurate modeling of individual LRGs are needed to resolve the satellite profile on the smallest scales. Such analyses would help determine whether the drop we find in the profile at $r < 15$ kpc is indeed real.

5.3. Dependence on Satellite Mass

The projected number-density profile can be further utilized to study the distribution of mass in LRG halos. We divided our sample of detected objects into three luminosity bins (assuming all objects are at the same redshift as the LRG in their field) and repeated the statistical number-density profile extraction for each bin. Figure 4 shows the resulting profiles of the most luminous, intermediate-luminosity, and faintest satellite galaxies (orange, green, and blue lines, respectively). In the top panel, the relative contributions of each luminosity bin is presented, as well as the overall profile of all satellites (solid red line). In the (linearly rescaled) bottom panel we normalized the three profiles to the intermediate-luminosity bin based on the curve value at $r \sim 200$ kpc.

Figure 4 shows that at $r > 25$ kpc the normalized profiles agree remarkably well with each other while at smaller radii the fraction of bright satellite galaxies increases. The good agreement between the three luminosity bins in the range $25 < r/\mathrm{kpc} < 700$ suggests that a strong mass segregation of LRG satellites does not exist. We also note that in this range the overall number-density profile is dominated by the dark matter halo (Figure 3). At radii smaller than 25 kpc, where baryons dominate the gravitational potential, the fraction of luminous satellites seems to increase. A naive interpretation would suggest that as satellite galaxies get closer to the central LRG, the probability of retaining their stars is proportional to their initial mass. However, since the difference between the three luminosity bins is only pronounced in the innermost parts of the profile, we conclude that our results are consistent with only a mild mass segregation in LRG environments.

5.4. Sources of Uncertainty

Throughout this Letter we utilize a key assumption that satellite galaxies around LRGs are an unbiased tracer of the total mass distribution. However, it is known that halos, especially at the high-mass end of the mass function, continue to evolve and are not in dynamical equilibrium (e.g., Bell et al. 2006; Wake et al. 2008; Tal et al. 2009; van Dokkum et al. 2010; Tojeiro & Percival 2011; Skelton et al. 2011). This implies that measurements of projected satellite radii (and therefore the number-density profile) may potentially be dominated by, e.g., the trajectories of infalling systems. Estimates of the dynamical state of LRG halos are important for proper assessment of our results but are unfortunately beyond the scope of this Letter.

Furthermore, we note that our measurement of background and foreground sources was not extracted from truly random fields. The random apertures which we used to derive this measurement were positioned along the same SDSS fields as the LRG apertures to match the photometric properties of the fields

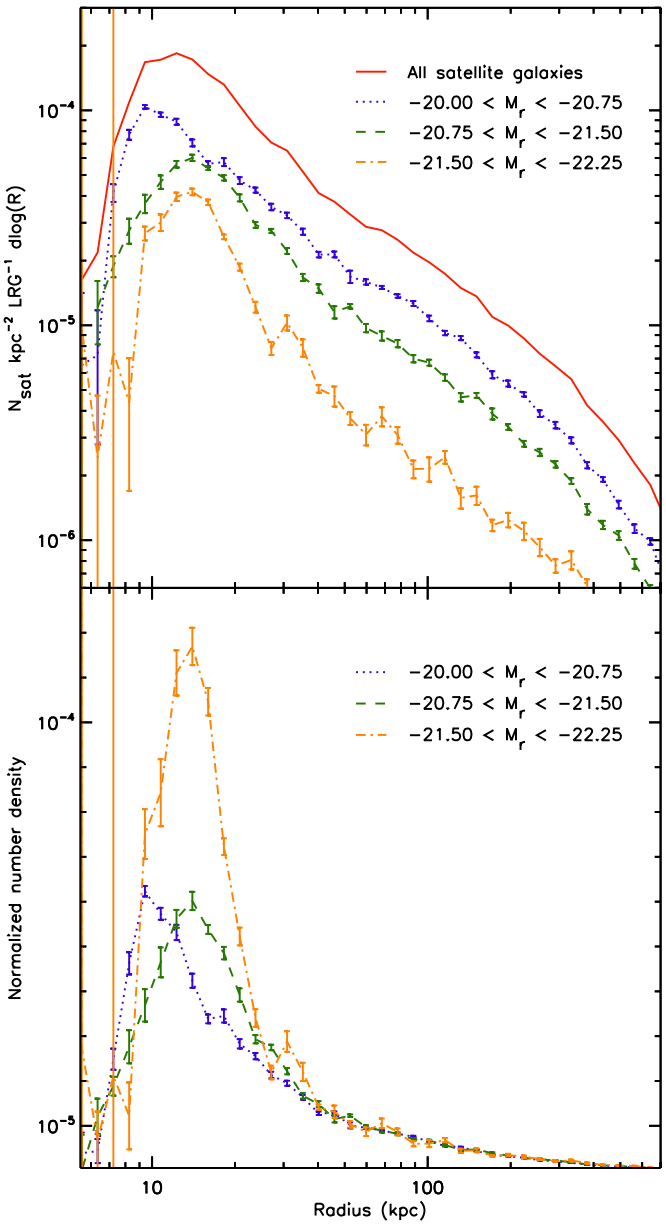

Figure 4. Projected number-density profiles of LRG satellites binned by luminosity. Top panel: the solid red line shows the overall profile of all satellite galaxies. Dotted purple, dashed green, and dot-dashed orange lines show the radial satellite distribution of the faintest, intermediate-luminosity, and most luminous galaxies, respectively. Bottom panel: the three profiles are normalized to the intermediate-luminosity bin according to their $r \sim 200$ kpc data point. While the three curves agree in the range $25 < r/\mathrm{kpc} < 700$, the fraction of luminous satellites increases significantly at small projected radii. All lines are plotted in log-linear scale to enhance the difference between the profiles.

(A color version of this figure is available in the online journal.)

and to sample the large-scale structure around the LRG halos. This implies that some satellite galaxies were possibly included in the random aperture catalogs, resulting in an oversubtraction of background and foreground sources, especially at large radii.

An additional source of uncertainty stems from our selection of the model fitting range. In order to test how the best-fit scale radius of the NFW profile depends on the choice of fitting boundaries we varied the lower threshold radius between 10 and 25 kpc and repeated the NFW+Sérsic model fitting procedure. The resulting scale radius was found to be in the range $240 < r_s/\mathrm{kpc}/270$ and the stellar conversion efficiency remained in the range $0.030 < \eta < 0.037$. The small variation in derived r_s and η suggests that the number-density profile is only mildly sensitive to the choice of lower fitting limit.

The magnitude threshold used for source extraction also affects the resulting best-fit model parameters. To test this we extended our analysis to fainter satellites and found that the dark-to-baryonic mass ratio increases by up to 20% when the extraction limit is set to 22 mag. However, we note that the detection fraction of sources in this brightness range drops to under 70% at large radii and to roughly 50% at $r = 15$ kpc. This suggests that the above-mentioned increase in the value of dark-to-baryonic mass ratio is likely dominated by underestimates of the number density of faint satellites.

Finally, the physical processes that affect satellite galaxies at small radii (such as tidal stripping) may also influence galaxies, to a lesser degree, everywhere else in the group or cluster. This means that satellites may become fainter as they gradually move closer to the central LRG. Such satellites are more likely to fall under the detection threshold with decreasing radius, thus making the number-density slope overall shallower.

We gratefully acknowledge support from the CT Space Grant. This letter is based on data from the Sloan digital sky survey.

REFERENCES

Abazajian, K. N., Adelman-McCarthy, J. K., Agüeros, M. A., et al. 2009, ApJS, 182, 543
Bartelmann, M. 1996, A&A, 313, 697
Bell, E. F., Naab, T., McIntosh, D. H., et al. 2006, ApJ, 640, 241
Bertin, E., & Arnouts, S. 1996, A&AS, 117, 393
Bolton, A. S., Burles, S., Koopmans, L. V. E., Treu, T., & Moustakas, L. A. 2006, ApJ, 638, 703
Bolton, A. S., Treu, T., Koopmans, L. V. E., et al. 2008, ApJ, 684, 248
Fabricant, D., Lecar, M., & Gorenstein, P. 1980, ApJ, 241, 552
Fadda, D., Girardi, M., Giuricin, G., Mardirossian, F., & Mezzetti, M. 1996, ApJ, 473, 670
Forman, W., & Jones, C. 1982, ARA&A, 20, 547
Gavazzi, R., Treu, T., Rhodes, J. D., et al. 2007, ApJ, 667, 176
Girardi, M., Biviano, A., Giuricin, G., Mardirossian, F., & Mezzetti, M. 1993, ApJ, 404, 38
Guo, Q., Cole, S., Eke, V., & Frenk, C. 2012, arXiv:1201.1296
Madore, B. F., Freedman, W. L., & Bothun, G. D. 2004, ApJ, 607, 810
Mandelbaum, R., Seljak, U., Kauffmann, G., Hirata, C. M., & Brinkmann, J. 2006, MNRAS, 368, 715
Markwardt, C. B. 2009, in ASP Conf. Ser. 411, Astronomical Data Analysis Software and Systems XVIII, ed. D. A. Bohlender, D. Durand, & P. Dowler (San Francisco, CA: ASP), 251
Masjedi, M., Hogg, D. W., & Blanton, M. R. 2008, ApJ, 679, 260
Masjedi, M., Hogg, D. W., Cool, R. J., et al. 2006, ApJ, 644, 54
Mulchaey, J. S. 2000, ARA&A, 38, 289
Mulchaey, J. S., Davis, D. S., Mushotzky, R. F., & Burstein, D. 1993, ApJ, 404, L9
Navarro, J. F., Frenk, C. S., & White, S. D. M. 1996, ApJ, 462, 563
Navarro, J. F., Frenk, C. S., & White, S. D. M. 1997, ApJ, 490, 493
Nierenberg, A. M., Auger, M. W., Treu, T., Marshall, P. J., & Fassnacht, C. D. 2011, ApJ, 731, 44
Reid, B. A., & Spergel, D. N. 2009, ApJ, 698, 143
Sales, L. V., Navarro, J. F., Lambas, D. G., White, S. D. M., & Croton, D. J. 2007, MNRAS, 382, 1901
Skelton, R. E., Bell, E. F., & Somerville, R. S. 2011, arXiv:1112.1077
Tal, T., & van Dokkum, P. G. 2011, ApJ, 731, 89
Tal, T., van Dokkum, P. G., Nelan, J., & Bezanson, R. 2009, AJ, 138, 1417
Tal, T., Wake, D. A., van Dokkum, P. G., et al. 2012, ApJ, 746, 138
Tojeiro, R., & Percival, W. J. 2011, MNRAS, 417, 1114
Vader, J. P., & Sandage, A. 1991, ApJ, 379, L1
van den Bosch, F. C., Yang, X., Mo, H. J., & Norberg, P. 2005, MNRAS, 356, 1233
van Dokkum, P. G., Whitaker, K. E., Brammer, G., et al. 2010, ApJ, 709, 1018
Vikhlinin, A., Kravtsov, A., Forman, W., et al. 2006, ApJ, 640, 691
Wake, D. A., Sheth, R. K., Nichol, R. C., et al. 2008, MNRAS, 387, 1045
Watson, D. F., Berlind, A. A., McBride, C. K., Hogg, D. W., & Jiang, T. 2011, arXiv:1108.1195
York, D. G., Adelman, J., Anderson, J. E., Jr., et al. 2000, AJ, 120, 1579
Zehavi, I., Blanton, M. R., Frieman, J. A., et al. 2002, ApJ, 571, 172
Zheng, Z., Zehavi, I., Eisenstein, D. J., Weinberg, D. H., & Jing, Y. P. 2009, ApJ, 707, 554